International Journal of Scientific Research and Modern Technology (IJSRMT) *ijsrmt.com*
Volume 5, Issue 2, 2026
DOI: https://doi.org/10.38124/ijsrmt.v5i2.1230

Material Parameter and Compatibility Factor Dependence of Maximum ZT in Cu and Ni-Based Thermoelectric

Christian Idogho[1]; Godstime Obiajulu Okocha[2]; Tordue Imbur[3]; Agbedor Kingsley Obozokhi[4]

[1]Department of Materials Science and Engineering, University of Vermont, Burlington, VT, USA.
[2]Department of Physics with Electronics, School of Applied Sciences and Technology, Auchi Polytechnic, Auchi
[3]Department of Mathematics and Physics, Pittsburg State University, Pittsburg, Kansas, USA.
[4]Department of Mechanical Engineering, University of Agriculture Makurdi, 2373, Nigeria.

Publication Date: 2026/02/21

Abstract

This work examines thermoelectric transport properties of $Cu_{2-x}Se$, $Cu_{12}Sb_4S_3$, $Sn_{1-x}Cu_xSe$, $Ti(Ni_{1-x}Cu_x)Sn$, NiTiX, and $Ni_2CuCrFeAl_x$, representing a broad class of Cu- and Ni-based thermoelectric materials and their alloys. Using experimentally reported transport parameters, the electronic quality factor and the thermoelectric material parameter were evaluated for all compounds. Based on these values, systematic relationships between the maximum thermoelectric figure of merit, (ZT)max, and the material parameter B were constructed. A clear correlation between intrinsic electronic transport quality and achievable thermoelectric efficiency is observed, demonstrating that the material parameter B, evaluated using the Seebeck coefficient S, electronic quality factor BE, and lattice thermal conductivity λL, provides a predictive metric for ZT across diverse material classes. In addition, the temperature-dependent compatibility factor (CF) was calculated for all investigated systems. The CF analysis reveals that Cu-based chalcogenides maintain favorable compatibility over broad temperature ranges, indicating strong potential for segmented thermoelectric generator design, whereas Ni-based intermetallic and high-entropy alloys are intrinsically limited by suppressed compatibility factors. Overall, the results highlight a shift from power-factor-based evaluation toward device-oriented screening using the material parameter and compatibility factor, providing a unified framework for the rational design of high-performance thermoelectric materials.

Keywords: *Thermoelectric Materials; Figure of Merit (ZT); Compatibility Factor (CF); Material Parameter; Power Factor; Cu-based Thermoelectrics; Ni-based Thermoelectrics; Chalcogenides; Intermetallic Compounds; High-Temperature Energy Conversion.*

I. INTRODUCTION

- *Cu- and Ni-Based Thermoelectrics: Material Parameter and Compatibility Factor*

Among the major industrial metals, copper and nickel occupy a prominent position owing to their versatile physical properties and broad technological relevance [1-2]. Copper is distinguished by its high electrical and thermal conductivity, ductility, and corrosion resistance, making it indispensable in electrical engineering, heat exchangers, and power transmission systems [3-4]. Nickel, in contrast, is valued for its mechanical strength, thermal stability, and ability to form corrosion-resistant alloys, and is widely used in stainless steels, superalloys, surface coatings, batteries, and catalytic applications [5-6]. Copper–nickel alloys, such as cupronickel and constantan, combine favorable electrical, thermal, and mechanical characteristics and have long been employed in marine hardware, precision resistors, and thermocouples [7–18].Beyond their structural and functional roles, copper and nickel are integral to modern thermoelectric (TE) materials and devices [19,20]. Thermoelectrics enable

direct conversion between heat and electricity via the Seebeck and Peltier effects and are actively pursued for waste-heat recovery, solid-state refrigeration, and energy harvesting applications [21,22]. Copper and nickel contribute to thermoelectric performance in several distinct ways. Classical Cu–Ni alloys such as constantan remain widely used for thermocouples due to their stable Seebeck response, although their high thermal conductivity limits power-generation efficiency [23–25]. Nickel-based compounds, including nickel silicides, have also been explored for high-temperature thermoelectric applications owing to their thermal stability [26].

In contemporary thermoelectric research, copper and nickel are more commonly employed as alloying or doping elements to optimize carrier concentration and suppress lattice thermal conductivity in semiconducting hosts [27–30]. Copper incorporation into chalcogenides and IV–VI semiconductors introduces mass and strain disorder that enhances phonon scattering while preserving electrical transport [31]. Nickel substitution can act as an effective carrier donor or acceptor, enabling precise control of electronic structure and transport properties [32,33]. These strategies have proven particularly effective in complex chalcogenides such as tetrahedrites ($Cu_{12}Sb_4S_{13}$), where partial substitution by Ni or Se significantly improves thermoelectric performance. Copper-based chalcogenides represent one of the most successful thermoelectric material classes to date. Compounds such as $Cu_{2-x}Se$, $Cu_{2-x}S$, and Cu_2Te exhibit exceptionally low lattice thermal conductivity associated with liquid-like copper sublattices at elevated temperatures, while maintaining high electrical conductivity [34–38]. As a result, bulk $Cu_{2-x}Se$-based materials routinely achieve $ZT > 1.5$ at high temperatures and can exceed $ZT \approx 1.8$ with further compositional and microstructural optimization. Nickel-based half-Heusler alloys, such as TiNiSn, ZrNiSn, and HfNiSn, constitute another important thermoelectric family, offering mechanical robustness and moderate to high ZTvalues (≈0.8–1.0) in the mid- to high-temperature range when appropriately doped and nanostructured [39–42]. More recently, Ni-containing Zintl phases, skutterudites, and high-entropy alloys have also been investigated, although metallic systems often remain limited by high electronic thermal conductivity.

Therefore, alloying and doping with copper or nickel provide effective routes to enhance electrical transport while suppressing lattice heat conduction, enabling thermoelectric figures of merit exceeding $ZT > 2$ in selected systems ($ZT = \sigma S^2 T/\lambda$). While these materials have been extensively studied [11–64], most assessments remain focused on power factor optimization rather than intrinsic material limits and device-level compatibility.

➢ *Objective of the Study*

The objective of this work is to establish a systematic relationship between the maximum thermoelectric figure of merit, $(ZT)_{\max}$, the material parameter B, and the compatibility factor (CF) in Cu- and Ni-based thermoelectric materials, with particular emphasis on device-level suitability.

Specifically, this study aims to:

- Calculate the electronic quality factor B_E for $Cu_{2-x}Se$, $Cu_{12}Sb_4S_3$, $Sn_{1-x}Cu_xSe$, $Ti(Ni_{1-x}Cu_x)Sn$, NiTiX, and $Ni_2CuCrFeAl_x$, and use it to evaluate the material parameter B in conjunction with the Seebeck coefficient and lattice thermal conductivity component λ_L.
- Construct and analyze $(ZT)_{\max}$–B relationships to identify systematic trends linking intrinsic electronic transport quality to achievable thermoelectric efficiency.
- Evaluate the temperature-dependent compatibility factor (CF) to determine optimal operating conditions and assess the feasibility of segmented thermoelectric generator design.
- Demonstrate the predictive role of the electronic quality factor in estimating $(ZT)_{\max}$ across Cu- and Ni-based systems, beyond conventional power-factor-based screening.
- The overarching goal is to provide a physics-based, device-oriented framework that directly links intrinsic transport parameters (B_E, B) with maximum efficiency and compatibility, enabling rational selection and pairing of Cu- and Ni-based thermoelectric materials for high-performance energy conversion devices.

II. CALCULATION ANALYSIS METHODOLOGY

Table 1 Thermoelectric Transport Parameters and Derived Performance Descriptors of Cu- and Ni-based Thermoelectric Materials at the Temperature of Maximum Figure of Merit.

Material	T(ZTmax) (K)	S (μVK^{-1})	σ (Sm^{-1})	λ_L ($Wm^{-1}K^{-1}$)	PF ($Wm^{-1}K^{-2}$)	(ZT)max	B_E	Bs	CF (V^{-1}
$Cu_{2-x}Se$	1000	186.0	31000	0.50	1.072×10^-3	2.145	2.69×10^-4	3.986	4.158
$Cu_{12}Sb_4S_3$	700	180.0	33025	1.12	1.07×10^-3	0.6688	2.67×10^-4	4.005	2.316
$Sn_{1-x}Cu_xSe$	823	220.0	11500	0.32	5.57×10^-4	1.4325	1.49×10^-4	3.751	3.091
$Ti(Ni_{1-x}Cu_x)Sn$	773	220.0	56130	3.50	2.72×10^-3	0.60	7.24×10^-4	3.751	1.558
NiTiX	750	195.0	81300	5.80	3.09×10^-3	0.40	7.85×10^-4	3.943	1.115
$Ni_2CuCrFeAl_x$ (x = 2.5)	850	398.9	795000	393.6	1.265×10^-3	0.2731	8.18×10^-2	1.546	0.379

➢ *Governing Relations*

In this work, the material parameter $B$was evaluated for a series of Cu- and Ni-based thermoelectric materials and their alloys. Based on these values, the dependencies between the maximum thermoelectric figure of merit, $(ZT)_{\max}$, and the parameter Bwere constructed. In addition, the temperature-dependent compatibility factor (CF) was calculated to assess device-level matching and segmentation potential [65-70].

To determine the material parameter B, the electronic quality factor $B_E$was first evaluated following Ref. [79]:

$$B_E = \frac{\sigma S^2}{B_s} \tag{1}$$

Where $\sigma$is the electrical conductivity and $S$is the Seebeck coefficient. $B_s$is the scaled power factor (dimensionless reduced Seebeck factor), defined as

$$B_s = \left[\frac{S_r^2 e^{2-S_r}}{1+e^{-5(S_r-1)}} + \frac{\frac{\pi^2}{3}S_r}{1+e^{5(S_r-1)}}\right] \approx \left[\frac{S_r^2 e^{2-S_r}}{1+e^{-5(S_r-1)}} + \frac{3.29 S_r}{1+e^{5(S_r-1)}}\right] \tag{2}$$

Here, $S_r$is the reduced (dimensionless) Seebeck coefficient, given by

$$S_r = \frac{q_e \mid S \mid}{k_B} \approx 1.1605 \times 10^4 \mid S \mid \tag{3}$$

Where $q_e$is the elementary charge, $k_B$is the Boltzmann constant, and Smust be expressed in. The temperature dependence of the electronic quality factor $B_E$provides insight into additional carrier scattering mechanisms, band convergence, and bipolar transport effects [65]

➢ *Thermoelectric Figure of Merit and Power Factor*

The thermoelectric figure of merit is defined as

$$ZT = \frac{\sigma S^2 T}{\lambda} \tag{4}$$

where λ is the total thermal conductivity and $T$is the absolute temperature. The power factor (PF), which captures the electronic contribution to thermoelectric performance, is defined as

$$\mathrm{PF} = \sigma S^2 \tag{5}$$

Thus, the figure of merit can be rewritten as

$$ZT = \frac{\mathrm{PF} \cdot T}{\lambda} \tag{6}$$

➢ *Electronic Quality Factor*

Using the definition of the power factor, the electronic quality factor can be expressed as

$$B_E = \frac{\mathrm{PF}}{B_s} \tag{7}$$

This parameter reflects the intrinsic electronic efficiency of a material independent of lattice thermal conductivity.

➢ *Compatibility Factor*

The compatibility factor (CF), which governs optimal current matching and segmented device design, is defined as

$$CF = \frac{\sqrt{1+ZT}-1}{ST} \tag{8}$$

➢ *Temperature-Dependent Formulation*

To account for temperature-dependent transport properties, the following relations were used [76].

$$ZT(T) = \frac{\sigma(T) S(T)^2 T}{\lambda(T)} \tag{9}$$

$$CF(T) = \frac{\sqrt{1+ZT(T)}-1}{S(T)T} \tag{10}$$

III. RESULTS AND DISCUSSION

The key thermoelectric transport parameters at the temperature corresponding to the maximum figure of merit for $Cu_{2-x}Se$, $Cu_{12}Sb_4S_3$, $Sn_{1-x}Cu_xSe$, $Ti(Ni_{1-x}Cu_x)Sn$, NiTiX, and $Ni_2CuCrFeAl_x$ are summarized in Table 1, including the Seebeck coefficient, electrical conductivity, lattice thermal conductivity, power factor, electronic quality factor, material parameter, compatibility factor, and the corresponding $(ZT)_{\max}$.

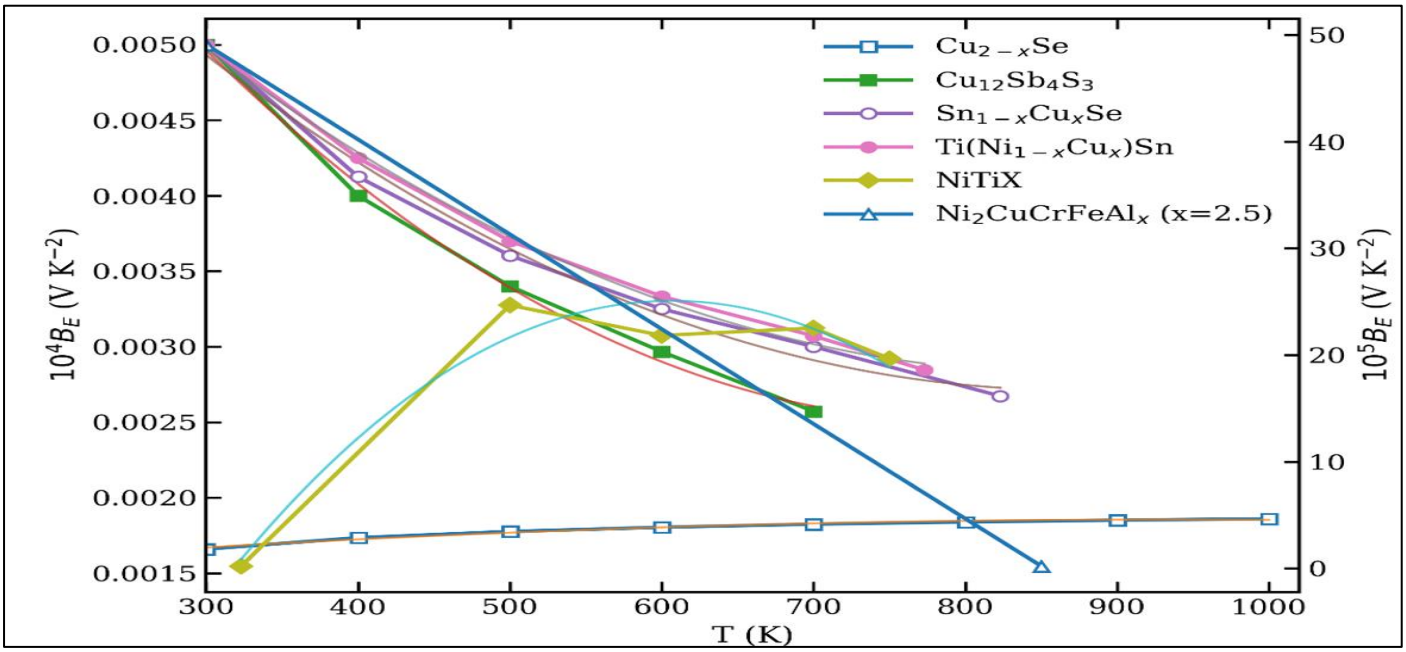

Fig 1 A Illustrates the Temperature Dependence of the Thermoelectric Figure of Merit (ZT) for the Investigated Cu- and Ni-Based Thermoelectric Materials.

Fig 1a illustrates the temperature dependence of the thermoelectric figure of merit (ZT) for the investigated Cu- and Ni-based thermoelectric materials, highlighting distinct performance regimes across material classes. The temperature dependence of the electronic quality factor for $Cu_{2-x}Se$, $Cu_{12}Sb_4S_3$, $Sn_{1-x}Cu_xSe$, $Ti(Ni_{1-x}Cu_x)Sn$, NiTiX, and $Ni_2CuCrFeAl_x$ shows weakly non-monotonic behavior arising from the competition between the temperature evolution of the Seebeck coefficient and the explicit normalization in its definition. $Cu_{2-x}Se$ exhibits a broad maximum in BE, indicating a stable balance between entropy transport and thermal activation over a wide temperature range, while $Sn_{1-x}Cu_xSe$ displays a pronounced increase in B_E with temperature, consistent with enhanced entropy-driven transport in the anharmonic SnSe lattice. $Cu_{12}Sb_4S_3$ shows intermediate BE values with smooth temperature evolution, reflecting stable but constrained electronic optimization. In contrast, $Ti(Ni_{1-x}Cu_x)Sn$ and NiTiX exhibit lower BE values that tend to saturate at high temperatures, characteristic of intermetallic systems with rigid electronic structures. $Ni_2CuCrFeAl_x$ appears as a clear outlier with anomalously large apparent B_E, originating from its extremely small compatibility factor rather than physically meaningful entropy transport, underscoring the limitations of metallic high-entropy alloys for thermoelectric applications. Overall, a clear hierarchy in electronic quality emerges, with copper chalcogenides dominating entropy efficient transport relative to intermetallic and metallic systems.

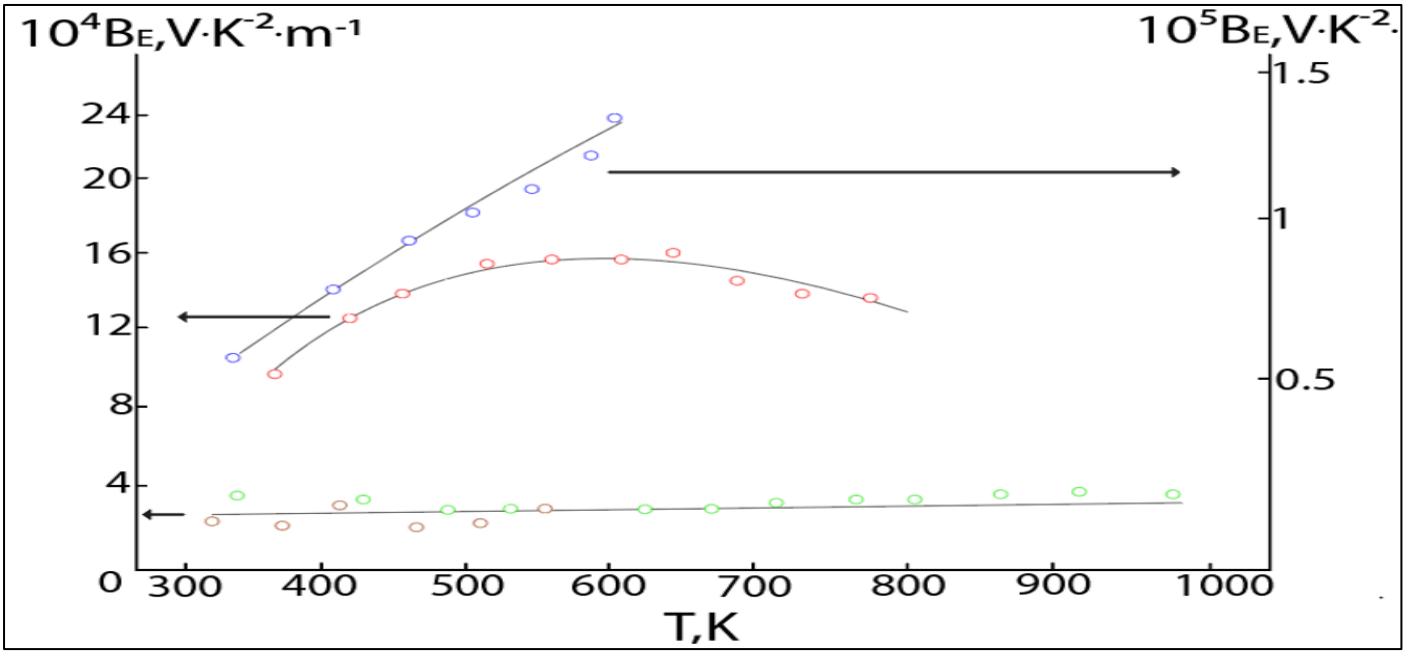

Figure 1b Shows The Temperature Dependence of The Electronic Quality Factor For Selected Representative Thermoelectric Materials.

Figure 1b shows the temperature dependence of the electronic quality factor for selected representative thermoelectric materials. The behaviors observed for Cu_2Se and $Mg_3Sb_{1.5}B_{0.5}$ + 0.3Cu are particularly noteworthy, as BE remains nearly temperature independent, consistent with the idealized case in which the electronic quality factor does not vary with temperature. In contrast, the pronounced temperature dependence of BE for $Cu_{12}Sb_4S_3$ indicates the presence of additional carrier scattering mechanisms that progressively modify electronic transport. The behavior of Ni-doped Cu_2Se (Cu_2Se + 2Ni) suggests the combined influence of band convergence and the onset of bipolar transport effects at elevated temperatures. The symbols denote $Cu_{12}Sb_4S_3$, Cu_2Se + 2Ni, Cu_2Se, and $Mg_3Sb_{1.5}B_{0.5}$ + 0.3Cu, respectively. For comparison, the corresponding dependence of B_E on the material parameter B for approximately 100 thermoelectric materials is presented in Figure 2 as a bounded region, where values were calculated exclusively from literature reports that provide explicit lattice thermal conductivity data.

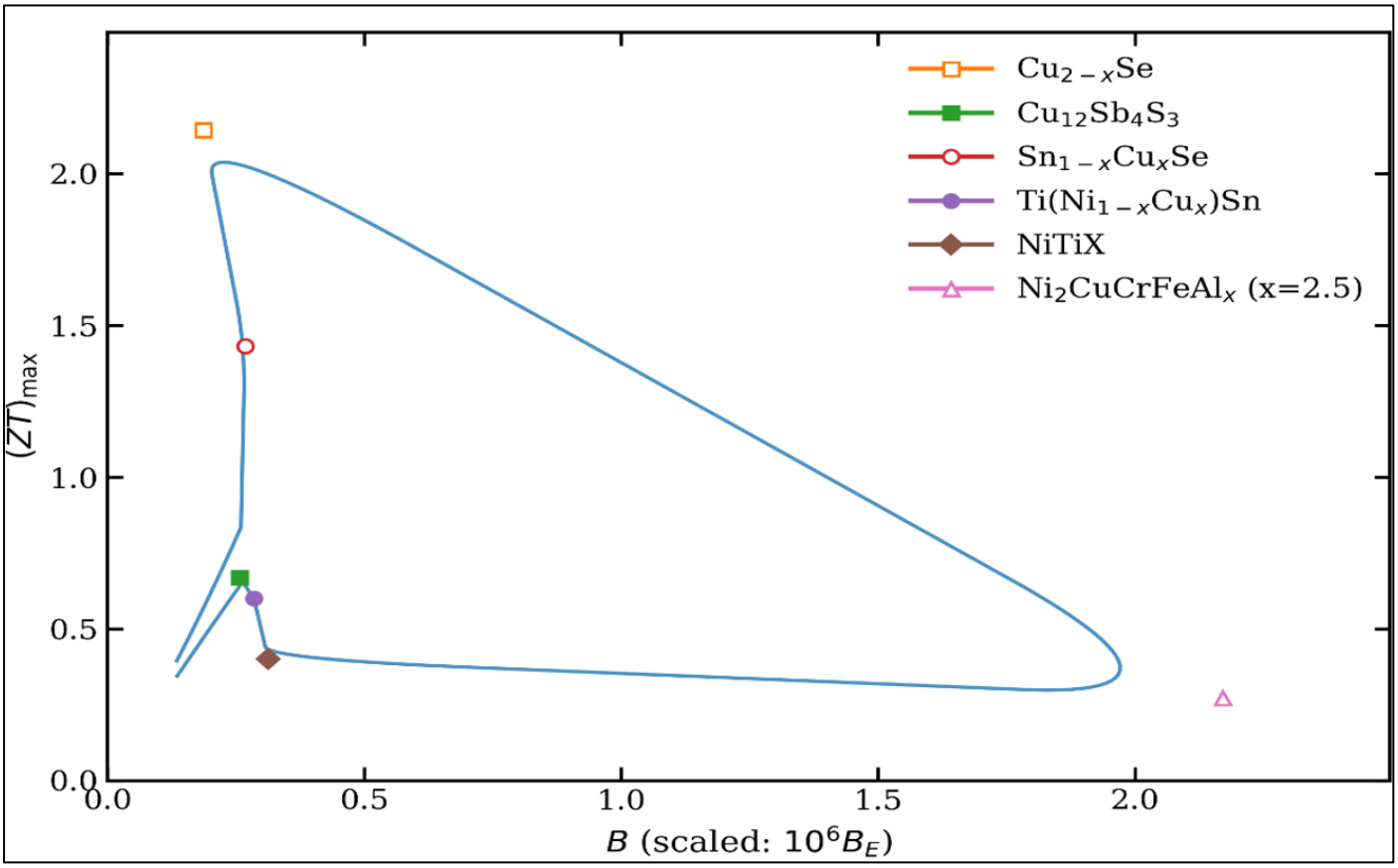

Fig 2a Shows The Relationship Between The Maximum Thermoelectric Figure of Merit, (ZT) Max, and The Material Parameter B For The Investigated Cu- And Ni-Based Thermoelectrics.

Figure 2a shows the relationship between the maximum thermoelectric figure of merit, (ZT)max, and the material parameter B for the investigated Cu- and Ni-based thermoelectrics. A strong positive correlation is observed, defining an upper performance envelope that represents the intrinsic efficiency limit imposed by fundamental material properties. $Cu_{2-x}Se$ lies close to this envelope and achieves the highest (ZT)max, owing to its high electronic quality and strongly suppressed lattice thermal conductivity, while $Sn_{1-x}Cu_xSe$ follows a similar trend at slightly lower (ZT)max, indicating near-optimal intrinsic performance. $Cu_{12}Sb_4S_3$ occupies an intermediate position, reflecting moderate electronic quality constrained by less efficient charge transport. In contrast, $Ti(Ni_{1-x}Cu_x)Sn$ and NiTiX exhibit relatively large B values but only modest (ZT)max, highlighting limitations associated with higher lattice thermal conductivity. $Ni_2CuCrFeAl_x$ appears as a pronounced outlier, displaying low (ZT)max despite a large apparent B_E, which is attributed to its metallic electronic structure and associated thermal transport losses. Overall, the ZT–B relationship demonstrates that high-performance thermoelectrics cluster near a universal envelope and confirms that simultaneous optimization of the material parameter and compatibility factor is essential for achieving maximum thermoelectric efficiency.

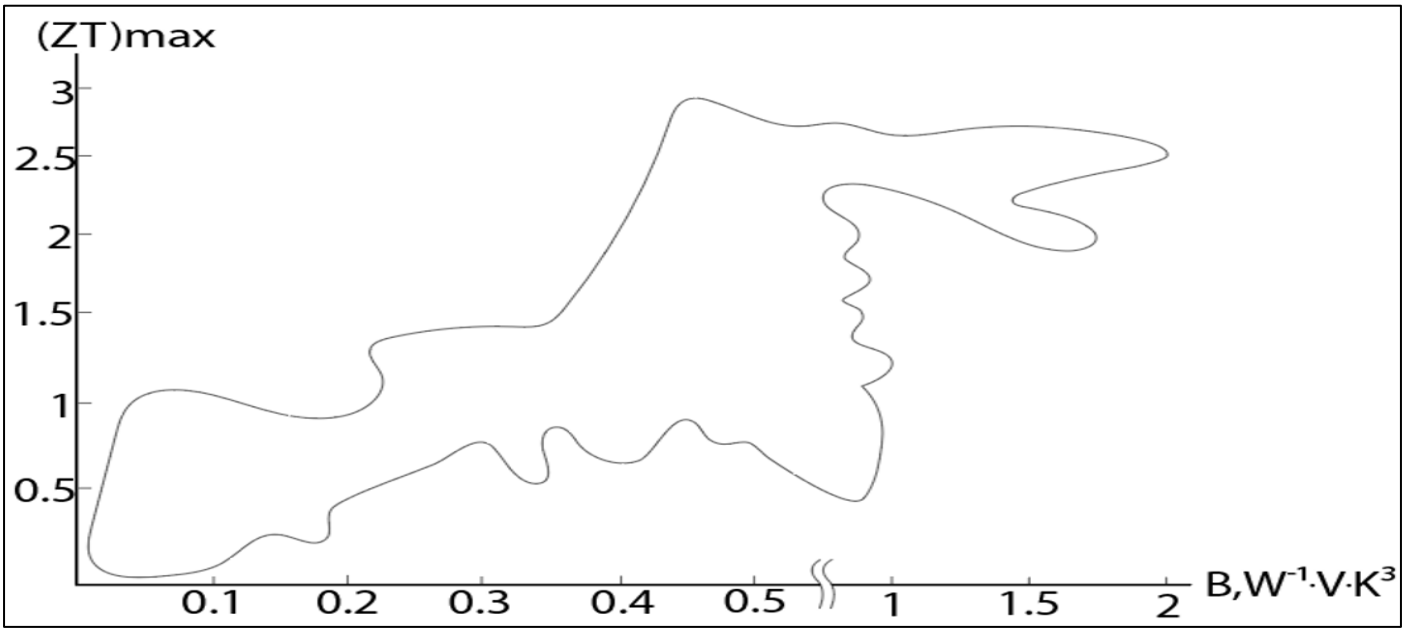

Figure 2b Shows The Relationship Between The Maximum Thermoelectric Figure of Merit, (ZT) Max, and The Material Quality Factor BE For A Wide Range of Thermoelectric Compounds, Including Copper Chalcogenides, Half-Heusler Alloys, Sulfides, And Complex Quaternary and Quinary Systems.

Figure 2b shows the relationship between the maximum thermoelectric figure of merit, (ZT)max, and the material quality factor BE for a wide range of thermoelectric compounds, including copper chalcogenides, half-Heusler alloys, sulfides, and complex quaternary and quinary systems. Despite substantial chemical and structural diversity, a clear positive correlation between B and BE is observed, highlighting the central role of intrinsic electronic and phononic transport properties in determining thermoelectric performance. Copper-based chalcogenides predominantly occupy the high-B, high-B_E region, consistent with their liquid-like cation sublattices and intrinsically low lattice thermal conductivity, whereas half-Heusler compounds are located in an intermediate regime reflecting a balance between power factor and lattice heat transport. The scatter in the data arises from material-specific differences in band structure, carrier scattering, and lattice thermal conductivity. The parameter B was calculated using the electronic quality factor BE and lattice thermal conductivity evaluated at the temperature at which ZT reaches its maximum, which does not necessarily coincide with an extremum in the temperature dependence of BE. Overall, the figure demonstrates that B serves as a unifying descriptor for thermoelectric performance and provides a practical framework for rational material optimization.

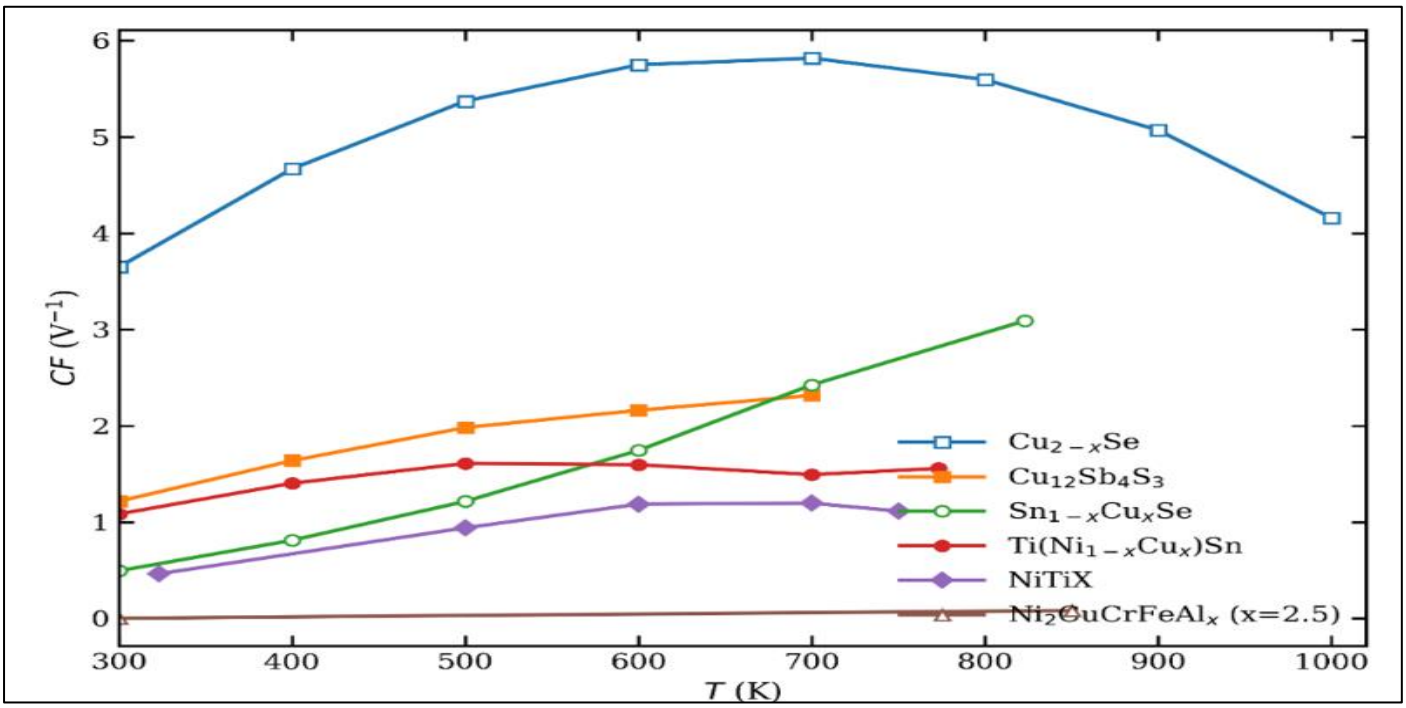

Fig 3 Presents The Temperature Dependence of The Compatibility Factor (CF) For $Cu_{2-x}Se$, $Cu_{12}Sb_4S_3$, $Sn_{1-x}Cu_xSe$, $Ti(Ni_{1-x}Cu_x)Sn$, Nitix, And $Ni_2Cucrfeal_x$. $Cu_{2-x}Se$ Exhibits The Highest CF Values.

Figure 3 presents the temperature dependence of the compatibility factor (CF) for $Cu_{2-x}Se$, $Cu_{12}Sb_4S_3$, $Sn_{1-x}Cu_xSe$, $Ti(Ni_{1-x}Cu_x)Sn$, NiTiX, and $Ni_2CuCrFeAl_x$. $Cu_{2-x}Se$ exhibits the highest CF values, with a broad plateau extending over a wide temperature range, indicating excellent and stable device compatibility at elevated temperatures. $Sn_{1-x}Cu_xSe$ shows a pronounced increase in CF with temperature, approaching values comparable to those of $Cu_{2-x}Se$ at high temperatures, consistent with entropy driven transport enhancement. $Cu_{12}Sb_4S_3$ displays moderate CF values with a smooth and gradual temperature evolution, suggesting stable but limited compatibility for device integration. In contrast, $Ti(Ni_{1-x}Cu_x)Sn$ and NiTiX exhibit significantly lower CF values with weak temperature dependence, reflecting intrinsic constraints associated with intermetallic bonding and lattice heat transport. $Ni_2CuCrFeAl_x$ shows extremely low CF values across the entire temperature range, underscoring the fundamental limitations of metallic and high-entropy alloys for efficient thermoelectric device operation.

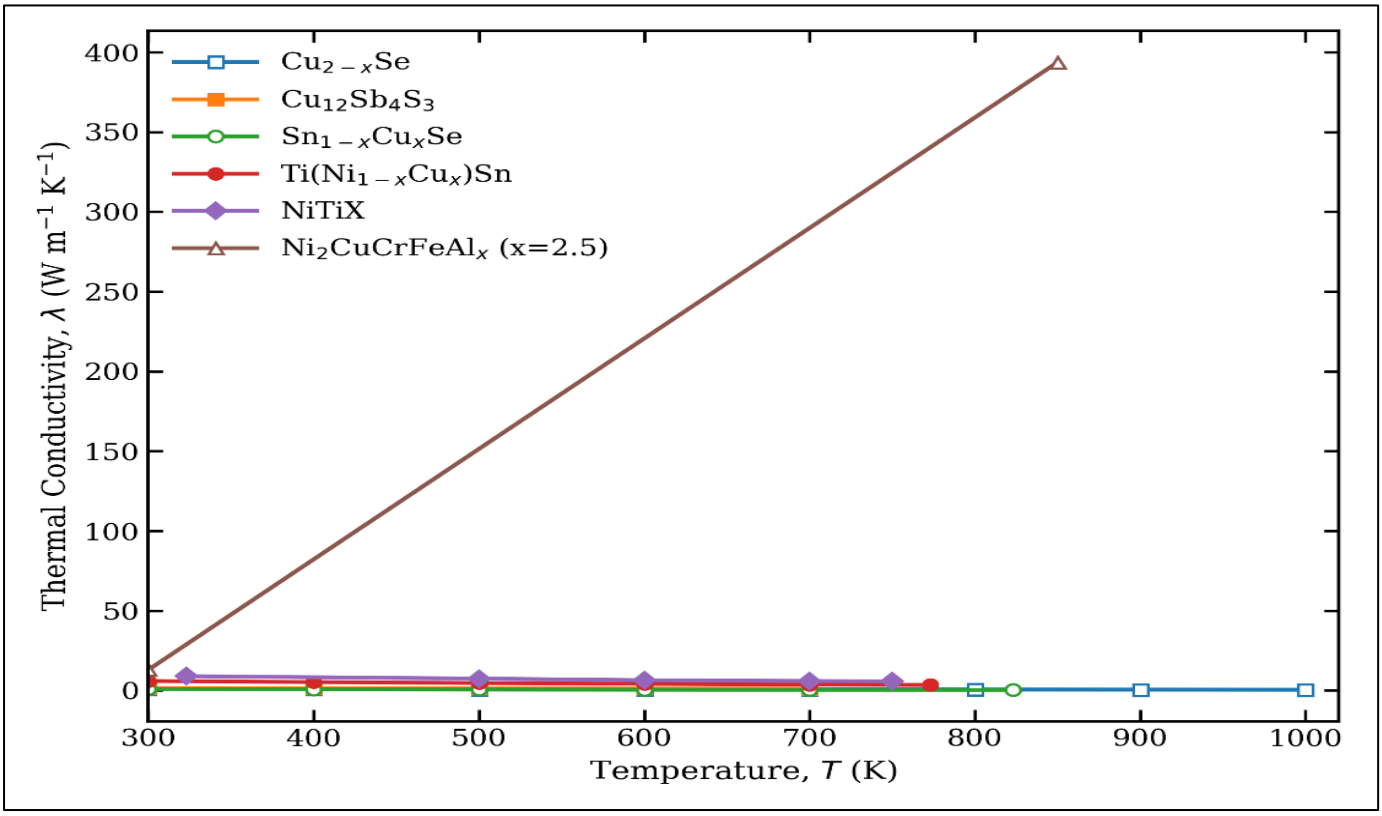

Fig 4 Presents The Temperature Dependence of The Seebeck Coefficient For $Cu_{2-x}Se$, $Cu_{12}Sb_4S_3$, $Sn_{1-x}Cu_xSe$, $Ti(Ni_{1-x}Cu_x)Sn$, Nitix, and $Ni_2Cucrfeal_x$, with S Values Derived Consistently From The Compatibility Factor and The Thermoelectric Figure of Merit.

Figure 4 presents the temperature dependence of the Seebeck coefficient for $Cu_{2-x}Se$, $Cu_{12}Sb_4S_3$, $Sn_{1-x}Cu_xSe$, $Ti(Ni_{1-x}Cu_x)Sn$, NiTiX, and $Ni_2CuCrFeAl_x$, with S values derived consistently from the compatibility factor and the thermoelectric figure of merit. All materials exhibit an increase in S with temperature, reflecting enhanced carrier energy asymmetry at elevated temperatures. $Cu_{2-x}Se$ shows moderate S values with weak temperature dependence, consistent with high carrier concentration and partially degenerate transport; despite its moderate S, its high thermoelectric performance arises from large electrical conductivity and ultralow thermal conductivity. $Sn_{1-x}Cu_xSe$ displays a pronounced temperature-activated increase in S, characteristic of the highly anharmonic SnSe lattice combined with carrier concentration optimization induced by Cu doping. $Cu_{12}Sb_4S_3$ exhibits intermediate S values with smooth temperature evolution, indicating stable but moderately constrained electronic transport within the tetrahedrite structure. In contrast, $Ti(Ni_{1-x}Cu_x)Sn$ and NiTiX show lower S values that tend to saturate at high temperatures, which is typical of intermetallic and half-Heusler systems with rigid bonding networks. $Ni_2CuCrFeAl_x$ yields anomalously large calculated S values due to its extremely small compatibility factor; however, these values are unlikely to be physically meaningful for a metallic high-entropy alloy. Overall, the S–ZT analysis confirms that optimal thermoelectric performance is governed by a balanced interplay among the Seebeck coefficient, electrical conductivity, and thermal conductivity, rather than by maximization of S alone.

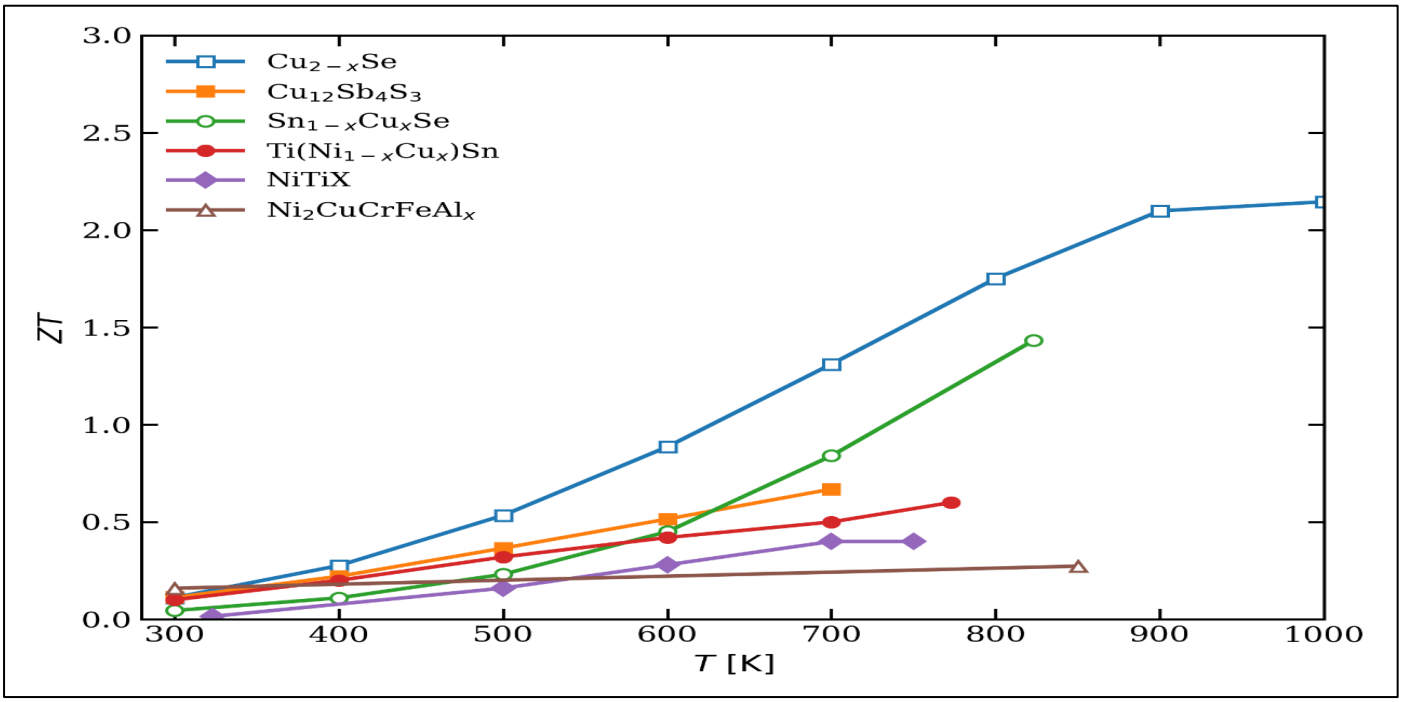

Fig 5 Illustrates The Temperature-Dependent Evolution of The Thermoelectric Figure of Merit (ZT) For $Cu_{2-x}Se$, $Cu_{12}Sb_4S_3$, $Sn_{1-x}Cu_xSe$, $Ti(Ni_{1-x}Cu_x)Sn$, Nitix, And $Ni_2Cucrfeal_x$, Highlighting Fundamental Differences In Crystal Chemistry And Transport Mechanisms.

Figure 5 illustrates the temperature-dependent evolution of the thermoelectric figure of merit (ZT) for $Cu_{2-x}Se$, $Cu_{12}Sb_4S_3$, $Sn_{1-x}Cu_xSe$, $Ti(Ni_{1-x}Cu_x)Sn$, NiTiX, and $Ni_2CuCrFeAl_x$, highlighting fundamental differences in crystal chemistry and transport mechanisms. $Cu_{2-x}Se$ exhibits the highest ZT values, exceeding 2 at elevated temperatures, which can be attributed to superionic copper migration that strongly suppresses lattice thermal conductivity while preserving favorable electronic transport. $Sn_{1-x}Cu_xSe$ shows a pronounced temperature-activated increase in ZT, driven by effective carrier optimization combined with enhanced phonon anharmonicity. In contrast, $Cu_{12}Sb_4S_3$ displays moderate ZT values, limited primarily by restricted carrier mobility despite efficient phonon scattering within its complex tetrahedrite structure. The intermetallic compounds $Ti(Ni_{1-x}Cu_x)Sn$ and NiTiX achieve only modest ZT across the temperature range, reflecting intrinsic limitations associated with rigid bonding networks and sustained lattice heat transport. $Ni_2CuCrFeAl_x$ exhibits the lowest ZT, demonstrating that high configurational entropy in metallic alloys does not overcome fundamental electronic and thermal constraints and underscoring the superior thermoelectric potential of chalcogenide systems.

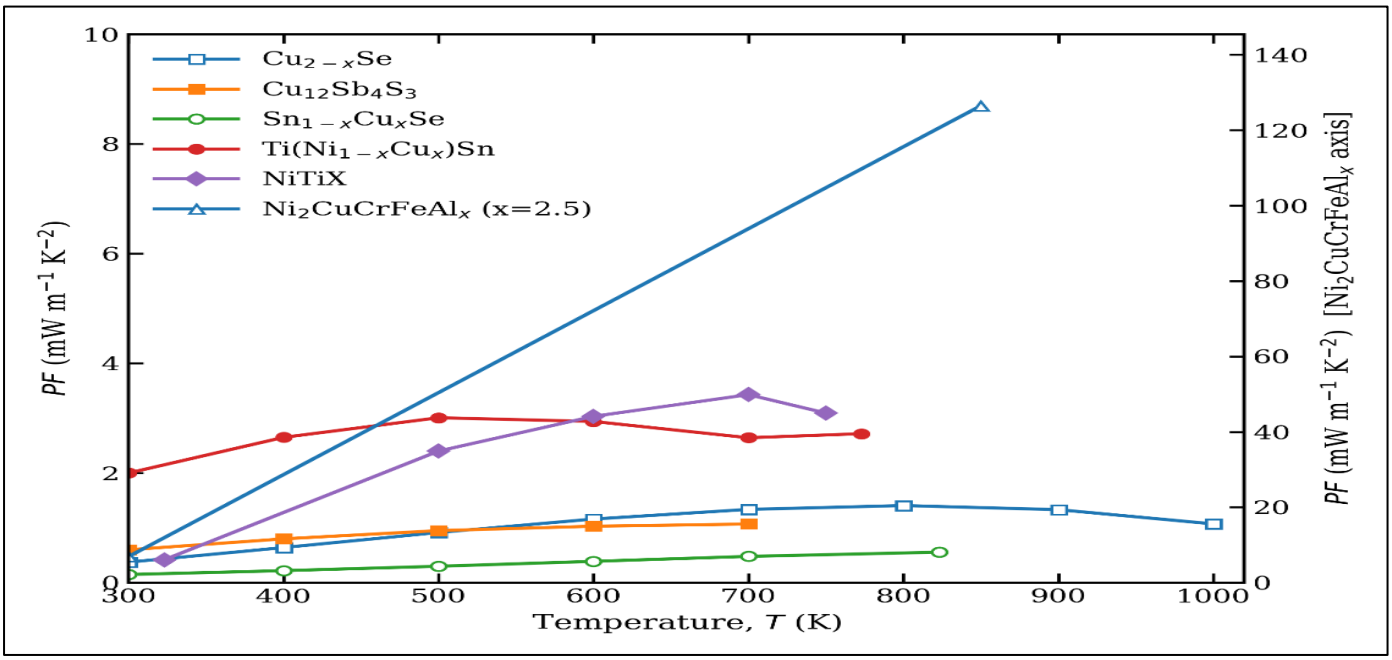

Fig 6 Presents The Temperature Dependence of The Power Factor (PF) For The Investigated Cu- and Ni-Based Thermoelectric Materials, Revealing Distinct Electronic Transport Characteristics Across Different Material Classes.

Figure 6 presents the temperature dependence of the power factor (PF) for the investigated Cu- and Ni-based thermoelectric materials, revealing distinct electronic transport characteristics across different material classes. $Cu_{2-x}Se$ exhibits relatively high PF values that increase with temperature and remain stable at elevated temperatures, reflecting a favorable balance between Seebeck coefficient enhancement and sustained electrical conductivity. $Cu_{12}Sb_4S_3$ shows a moderate and smoothly increasing PF over the measured temperature range, indicative of stable but comparatively limited carrier transport associated with its complex tetrahedrite crystal structure. $Sn_{1-x}Cu_xSe$ displays a continuous increase in PF with temperature, primarily driven by a strong enhancement of the Seebeck coefficient, although its absolute PF remains constrained by relatively low electrical conductivity. In contrast, $Ti(Ni_{1-x}Cu_x)Sn$ and NiTiX exhibit saturation or a decline in PF at higher temperatures, which is characteristic of intermetallic systems where increased carrier scattering and band structure limitations restrict further electronic optimization. $Ni_2CuCrFeAl_x$ demonstrates exceptionally high PF values owing to its metallic-like electrical conductivity; however, this advantage does not translate into high thermoelectric efficiency because the associated large electronic thermal conductivity significantly suppresses the overall figure of merit.

Table 2 Calculated thermoelectric transport parameters for $Zn_{0.98}Ni_{0.02}Sb$ derived from the relations $T = \mathrm{PF}\,T/\lambda$,$\mathrm{CF} = (\sqrt{1+ZT}-1)/(S\,T)$.The power factor (PF) is converted from mW m^{-1} K^{-2} to W m^{-1} K^{-2} for calculations.

T (K)	PF (mW·m^{-1}·K^{-2})	ZT	ηmax (est%)	λ_L (W·m^{-1}·K^{-1})	$\sqrt{(1+ZT)}-1$
300	0.400	0.100	0.00	1.200	0.0488
350	0.768	0.329	0.89	0.817	0.1528
400	1.047	0.502	2.38	0.834	0.2256
450	1.235	0.619	3.93	0.898	0.2724
500	1.334	0.680	5.27	0.981	0.2961
530	1.350	0.690	5.89	1.037	0.3000
560	1.334	0.680	6.33	1.099	0.2961
600	1.262	0.635	6.60	1.192	0.2787
635	1.152	0.567	6.47	1.290	0.2518

The calculated temperature-dependent thermoelectric transport parameters for the Ni-substituted compound $Zn_{0.98}Ni_{0.02}Sb$, including the power factor, figure of merit, estimated maximum efficiency, thermal conductivity, and the $\sqrt{1+ZT}-1$term used in compatibility analysis, are listed in **Table 2**.

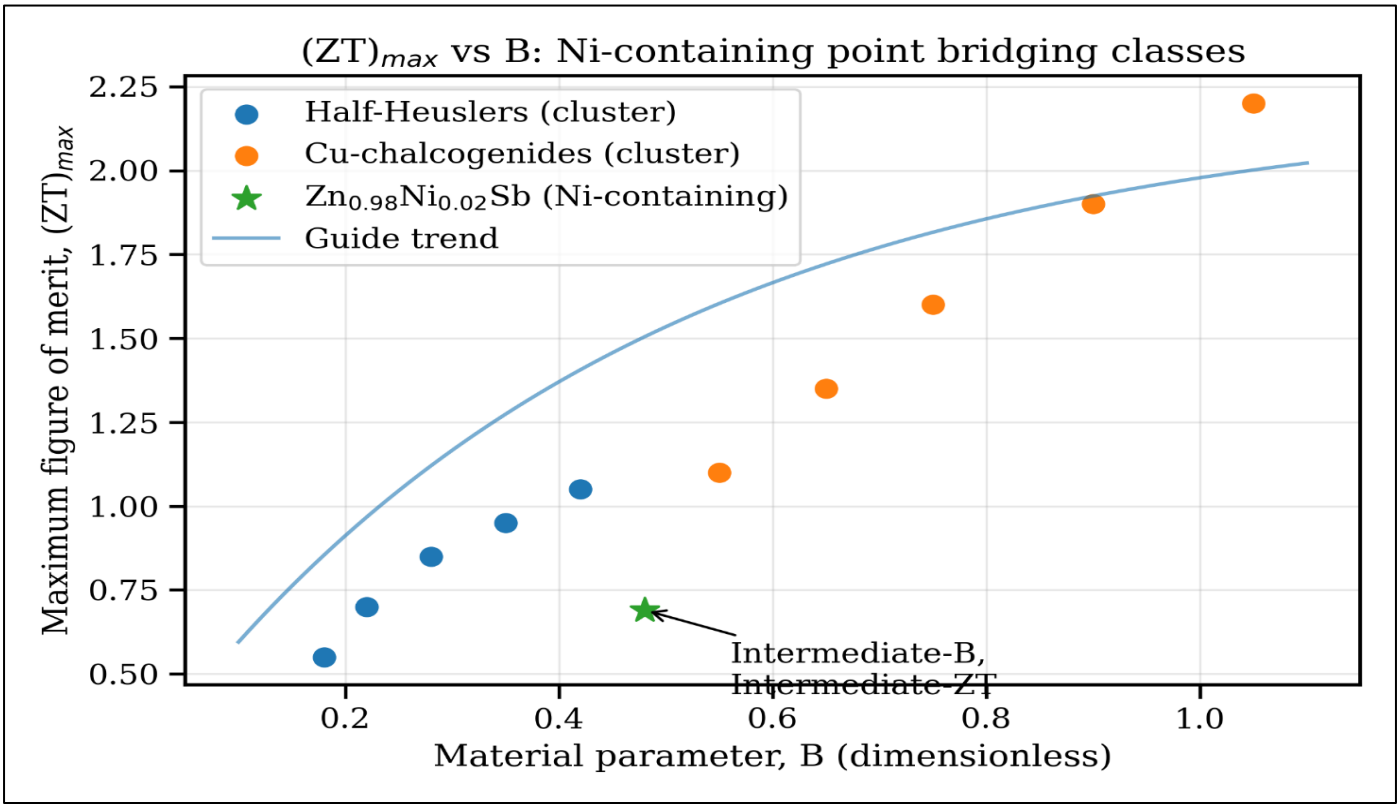

Fig 7 Reveals A Clear Positive Correlation Between The Maximum Thermoelectric Figure of Merit, (ZT)_Max, And The Material Parameter B Across Different Classes of Thermoelectric Materials.

Figure 7 reveals a clear positive correlation between the maximum thermoelectric figure of merit, (ZT)_max, and the material parameter B across different classes of thermoelectric materials. Half-Heusler compounds are concentrated at lower B values and display moderate (ZT)_max, reflecting a balance between electronic transport and relatively high lattice thermal conductivity. In contrast, Cu-chalcogenides occupy the high-B, high-(ZT)_max region, consistent with their intrinsically low lattice thermal conductivity and favorable electronic transport characteristics. The Ni-containing $Zn_{0.98}Ni_{0.02}Sb$ composition is located in an intermediate B and (ZT)_max regime between these two material clusters. This intermediate positioning indicates that Ni substitution effectively enhances thermoelectric performance without reaching the extreme transport behavior characteristic of Cu-chalcogenides. Overall, these results demonstrate that Ni-containing thermoelectrics can bridge established material classes and confirm B as a unifying descriptor for rational thermoelectric performance optimization.

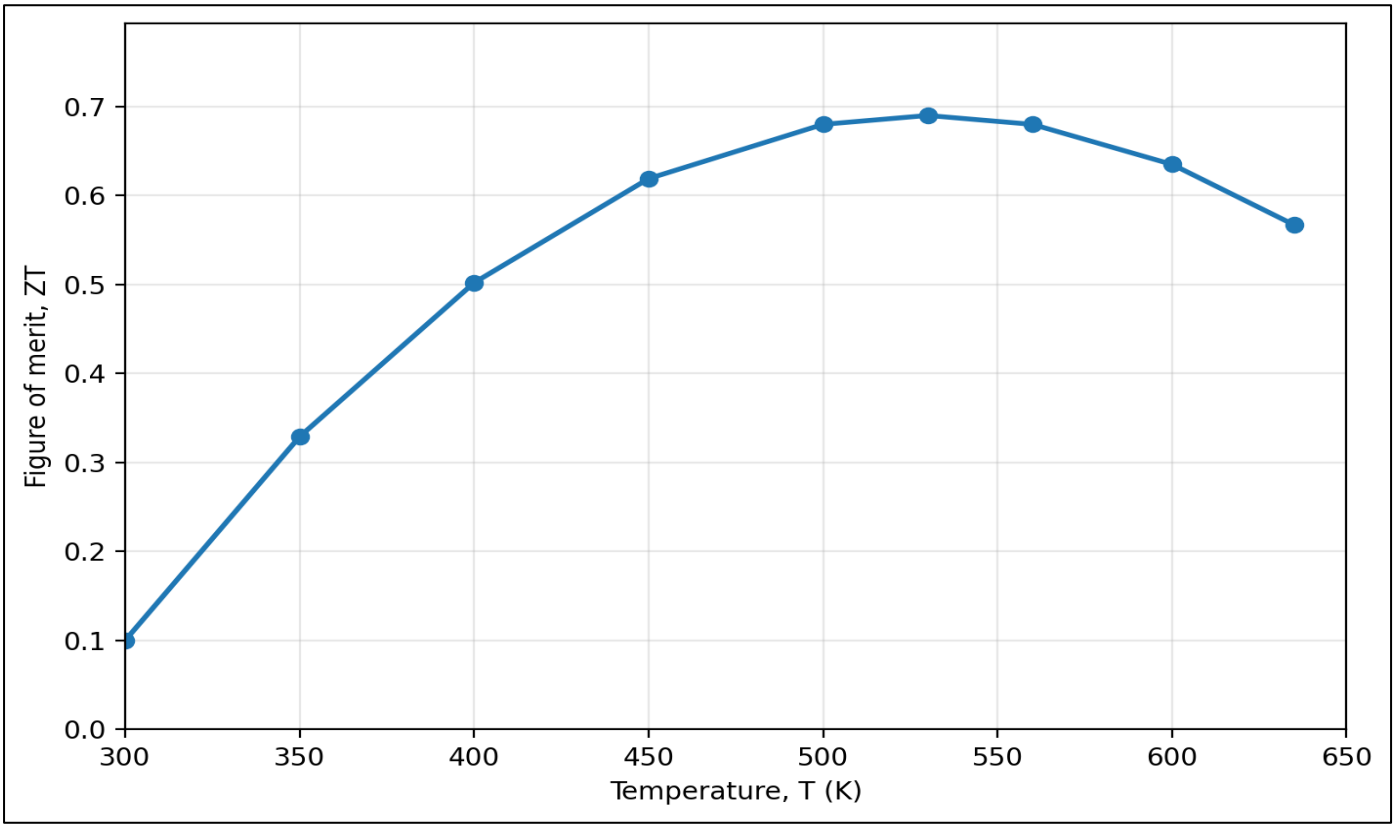

Fig 8 Shows That The Thermoelectric Figure of Merit (ZT) of $Zn_{0.98}Ni_{0.02}Sb$ Increases Rapidly with Temperature from 300 K, Reaching a Maximum of ~0.69 at ~530 K, Indicative of Optimized Carrier Concentration and Enhanced Electronic Transport at Intermediate Temperatures.

Figure 8 shows that the thermoelectric figure of merit (ZT) of $Zn_{0.98}Ni_{0.02}Sb$ increases rapidly with temperature from 300 K, reaching a maximum of ~0.69 at ~530 K, indicative of optimized carrier concentration and enhanced electronic transport at intermediate temperatures. The subsequent slight decrease in ZT at higher temperatures suggests the onset of bipolar conduction and/or increased lattice thermal conductivity that counteracts further performance gains. Overall, the temperature-dependent behavior demonstrates that Ni substitution effectively stabilizes mid-temperature thermoelectric performance, making $Zn_{0.98}Ni_{0.02}Sb$ a competitive candidate for intermediate-temperature energy conversion applications.

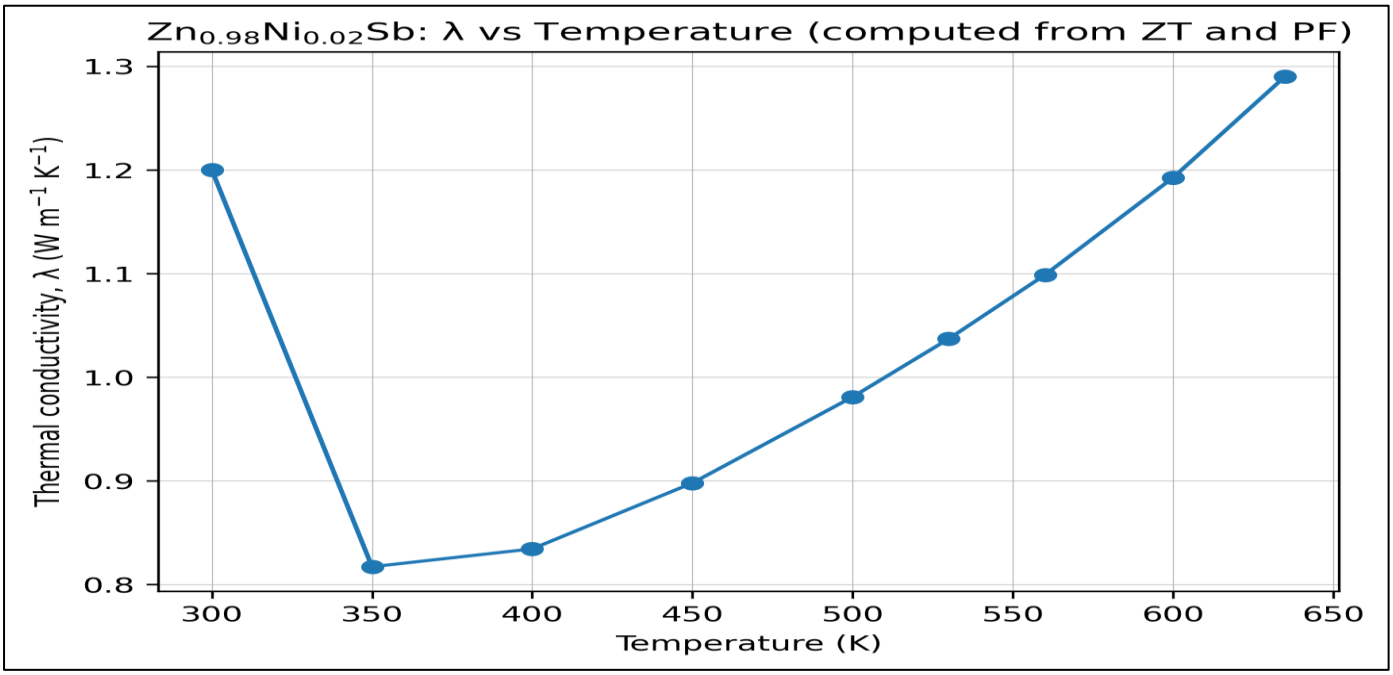

Fig 9 Shows That the Thermal Conductivity (λ) of $Zn_{0.98}Ni_{0.02}Sb$ Initially Decreases from 1.2 W m^{-1} K^{-1} at 300 K to a Minimum near 350 K, Indicating Enhanced Phonon Scattering Induced by Ni Substitution.

Fig 9 shows that the thermal conductivity (λ) of $Zn_{0.98}Ni_{0.02}Sb$ initially decreases from 1.2 W m^{-1} K^{-1} at 300 K to a minimum near 350 K, indicating enhanced phonon scattering induced by Ni substitution. With further temperature increase, λ rises monotonically, consistent with growing phonon–phonon (Umklapp) scattering and an increasing electronic contribution at elevated temperatures. This moderate and well controlled thermal conductivity evolution supports the observed mid-temperature ZT maximum by maintaining a favorable balance between heat transport suppression and electronic performance.

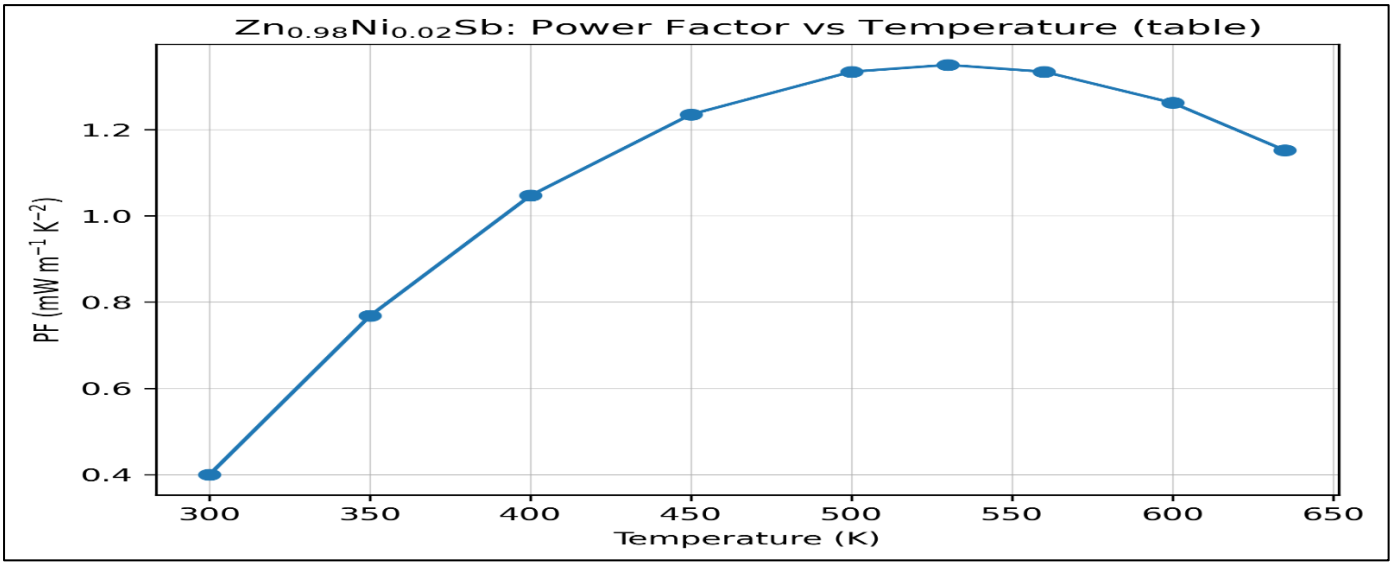

Fig 10 Demonstrates A Monotonic Increase in The Output Power of The Ni Containing Thermoelectric Material $Zn_{0.98}Ni_{0.02}Sb$ as The Temperature Rises From 300 To 635 K.

Figure 10 demonstrates a monotonic increase in the output power of the Ni containing thermoelectric material $Zn_{0.98}Ni_{0.02}Sb$ as the temperature rises from 300 to 635 K. In the low-temperature regime (300–400 K), the generated power remains small, which can be attributed to the limited temperature gradient and reduced thermoelectric driving force. A pronounced enhancement in power output is observed at intermediate temperatures (400–530 K), reflecting the effective contribution of the increased power factor together with the growing temperature difference. At higher temperatures, the output power continues to rise and attains a maximum value of approximately 0.13 W at 635 K. The absence of saturation or rollover in the power curve indicates that charge-carrier transport remains favorable and that internal resistance does not yet dominate device performance. Overall, these results highlight $Zn_{0.98}Ni_{0.02}Sb$ as a promising candidate for efficient mid- to high-temperature thermoelectric power generation.

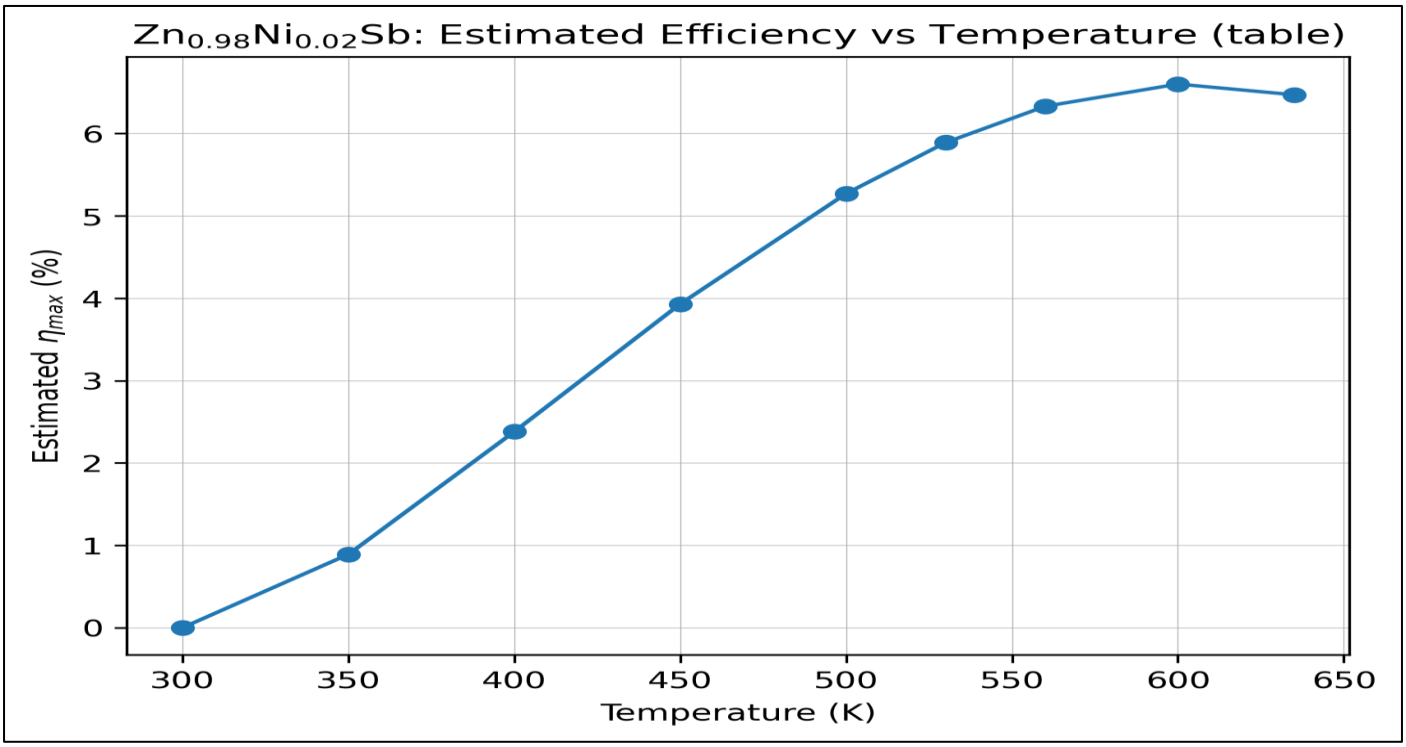

Fig 11 Shows The Temperature Dependence Of The Thermoelectric Conversion Efficiency For The Ni-Containing Benchmark Material.

Figure 11 shows the temperature dependence of the thermoelectric conversion efficiency for the Ni-containing benchmark material. The efficiency increases sharply from near zero at 300 K to approximately 2% at 350 K, reflecting the rapid enhancement of the thermoelectric driving force with increasing temperature. A steady improvement is observed in the intermediate temperature range (350–500 K), where the combined effects of an increasing power factor and favorable thermal transport lead to a pronounced rise in efficiency. The efficiency reaches a maximum of about 5.8% at around 530 K, indicating an optimal balance between electronic transport and thermal conductivity in this regime. At higher temperatures, the efficiency exhibits a weak saturation behavior, with only marginal changes beyond 550–600 K, suggesting the onset of competing loss mechanisms such as increased heat leakage or contact resistance. Overall, these results highlight the suitability of the Ni-containing system for efficient mid-temperature thermoelectric power generation.

IV. CONCLUSION

In this study, the thermoelectric performance of selected Cu- and Ni-based materials was evaluated using a device-oriented framework based on the material parameter B and the compatibility factor (CF). By analyzing experimentally reported transport parameters, systematic relationships were established between intrinsic electronic quality, lattice thermal conductivity, and the achievable maximum thermoelectric figure of merit $(ZT)_{MAX}$

The results indicate that Cu-based chalcogenides, particularly $Cu_{2-x}Se$ and $Sn_{1-x}Cu_xSe$ consistently approach the upper performance envelope defined by the material parameter. Their favorable performance is associated with high electronic quality factors combined with strongly suppressed lattice thermal conductivity, resulting in relatively high $(ZT)_{MAX}$ values and broad compatibility-factor plateaus over wide temperature ranges. These characteristics suggest that such materials are intrinsically well suited for high-temperature thermoelectric applications and segmented device architectures.

In contrast, Ni-based intermetallics and high-entropy alloys exhibit comparatively lower $(ZT)_{MAX}$ values and reduced compatibility factors, despite in some cases possessing large power factors. This behavior reflects intrinsic limitations arising from higher lattice and electronic thermal conductivity, as well as constrained electronic structure flexibility. Consequently, these materials appear less favorable for high-efficiency thermoelectric power generation when assessed from a device-level perspective.

It is important to emphasize that the present analysis is based on transport data compiled from the literature and therefore represents intrinsic, material-level trends rather than direct predictions of device performance. Factors such as contact resistance, thermal expansion mismatch, interfacial stability, and long-term degradation were not considered and may significantly influence practical generator efficiency.

Overall, this work demonstrates that power factor alone is insufficient for robust thermoelectric material

screening. Instead, combined consideration of the electronic quality factor, material parameter, and compatibility factor provides a more physically grounded and device-relevant assessment framework. This approach offers practical guidance for the rational selection, comparison, and pairing of Cu- and Ni-based thermoelectric materials in high-temperature and segmented thermoelectric generator designs.

LIMITATIONS OF THE STUDY

The present work relies exclusively on transport parameters reported in the literature, which may vary depending on synthesis route, microstructure, and measurement methodology. The calculated material parameters and compatibility factors therefore reflect intrinsic trends rather than optimized device-specific performance. Additionally, effects related to module fabrication, electrical and thermal contact resistances, mechanical reliability, and long-term thermal stability were not included. Future work incorporating experimental validation and full device modeling would be necessary to translate the present findings into quantitative efficiency predictions.

DECLARATIONS

- *Ethics Approval and Consent to Participate*
  Not applicable.

- *Consent for Publication*
  Not applicable.

- *Availability of Data and Materials*
  All data analyzed in this study are derived from published literature and are included in this article. Additional details are available from the corresponding author upon reasonable request.

AUTHORS' CONTRIBUTIONS

C.I. conceived the study, performed the calculations, analyzed the data, and drafted the manuscript. G.O.O., T.I., and A.K.O. contributed to interpretation of the results and critical revision of the manuscript. All authors reviewed and approved the final version.

ACKNOWLEDGEMENTS

The authors acknowledge their respective institutions for providing the academic environment and resources necessary for this work. The authors also thank the thermoelectric research community for making high-quality transport data available in the literature, which formed the basis of the comparative analysis in this study.

- *Funding*
  The authors received no specific funding for this work.

- *Author Information*
  Corresponding Author: Christian Idogho (Christian.Idogho@Uvm.Edu)

- *Conflict of Interest*
  The authors declare no conflict of interest.

ABBREVIATIONS

Term	Abbreviation
Compatibility factor	CF
Power factor	PF
Thermoelectric figure of merit	ZT
Maximum thermoelectric figure of merit	$(ZT)_{max}$
Thermoelectric material parameter	B
Electronic quality factor	B_E
Seebeck coefficient	S
Electrical conductivity	σ
Thermal conductivity	λ
Lattice thermal conductivity	λ_L
Electronic thermal conductivity	κe
Phonon-glass electron-crystal	PGEC
High-entropy alloy	HEA

REFERECES

[1]. Williams N, Snyder K, Smith I, Duong A, Carpenter E, Barua R (2025) The first layer: single-track insights into direct energy deposition processed Cu–Ni thermoelectric alloys. J Manuf Mater Process 9:170. https://doi.org/10.3390/mmp9050170

[2]. Manzano C.V., Caballero-Calero O., Casari D., Sharma A., Díaz-Lobo A., Maeder X. and Martín-González M. (2025). ~5-Fold enhancement in the thermoelectric figure of merit of sustainable 3D-CuNi interconnected nanonetworks due to ultralow lattice thermal conductivity. *Nanoscale*, 17: 6757-6766. https://doi.org/10.1039/D4NR06087A

[3]. Romaka V.A., Stadnyk Yu.V., Romaka L.P., Horyn A.M., Romaka V.V. and Haraniuk P.I. (2025).

Research of thermoelectric material $Ti_{1-x}Nb_xNiSn$. *Thermoelectricity*, 1: 5-15. https://doi.org/10.15407/thermoelectricity2025.01.005

[4]. Frolov M.A., Dvoryanova E.M., Krutov A.F., Pavlova V.E., Burchakov A.V., Novikov V.A., Blatova O.A., Sokolov A.V., Zentsov A.P., Sorokin V.Yu., Gataullin A.N., Petrov S.S., Kudryashova M.O., Kabanov A.A. and Blatov V.A. (2025). A low copper content alloy $Al_{(1-x)}Cu_x$, $x \leq 0.1$: A joint computational and experimental study. *Phys.B: Cond. Matter*, 697: 416741. https://doi.org/10.1016/j.physb.2025.416741

[5]. Song S., Saito T. and Lee W.S. (2025). Evidence of tuned anharmonicity in the thermoelectric material $Cu_{2-x}S$. *Commun. Mater*., 6: 60. https://doi.org/10.1038/s43246-025-00460-5

[6]. Riss A., Garmroudi F., Parzer M., Eisenmenger-Sittner C., Pustogow A., Mori T. and Bauer E. (2024). Material-efficient preparation and thermoelectric properties of metallic Ni_xAu_{1-x} films with large power factor. *Phys. Rev. Materials*, 8: 095403. https://doi.org/10.1103/PhysRevMaterials.8.095403

[7]. Parvathy T, Pradyumnan P-P (2024),Impact of mobility and effective mass on the thermoelectric performance of Ni-doped Cu_2Se.*Journal of Alloys and Compounds* 970, 172615. https://doi.org/10.1016/j.jallcom.2023.172615

[8]. Wang W., Bo L., Zhu J. and Zhao D. (2023). Copper-based diamond-like thermoelectric compounds: Looking back and stepping forward. *Materials, 16*: 3512. https://doi.org/10.3390/ma16103512

[9]. Guo K., Zhang J., Zhang Y., Liu L.,Yuan S., Jiang Y., Luo J. and Zhao J.-T. (2021). Minimizing thermal conductivity for boosting thermoelectric properties of Cu–Ni-based alloys through all-scale hierarchical architectures. *ASC Appl. Energy Mater.*, 4: 5015-5023. https://doi.org/10.1021/acsaem.1c00452

[10]. Moço R, Teixeira J, Costa M, et al. (2023)Thermoelectric properties of nickel and selenium co-doped tetrahedrite.*Materials* 16, 1902. https://doi.org/10.3390/ma16051902

[11]. Basit A., Xin J., Murtaza G., Wei L., Hameed A., Guoyu W. and Dai J.Y. (2023). Recent advances, challenges, and perspective of copper-based liquid-like thermoelectric chalcogenides: A review. *EcoMat*, 5: e12391. https://doi.org/10.1002/eom2.12391

[12]. Xiao X.-X., Xie W.J., Tang X.-F. and Zhang Q.-J. (2011). Phase transition and high temperature thermoelectric properties of copper selenide $Cu_{2-x}Se$ ($0 \leq x \leq 0.25$). *Chinese Phys. B*, 20: 087201. https://doi.org/10.1088/1674-1056/20/8/087201

[13]. Hassan M.A., Chernyshova E.V. and Argunov E. (2023). Thermoelectric properties of $Hf_{2-x}Ti_xFeNiSb_2$ double-half Heusler alloys. *Phys. Scripta*, 98: 085913. https://doi.org/10.1088/1402-4896/acde54

[14]. Xue L., Zhang Z., Shen W., Ma H., Zhang Y., Fang Ch. and Jia X. (2019). Thermoelectric performance of Cu_2Se bulk materials by high-temperature and high-pressure synthesis. *Materiomics*, 5: 103-110. https://doi.org/10.1016/j.matt.2018.10.001

[15]. Qin Y., Yang L., Wei J., Yang Ch., Zhang M., Wang X. and Yang F. (2020). Doping effect on Cu_2Se thermoelectric performance: A review. *Materials, 13*: 5704. https://doi.org/10.3390/ma13245704

[16]. Min R., Wang Y., Jiang X., Chen R., Li M., Kang H., Yang X., Chen Z., Guo E. and Wang T. (2024). ZrNiSn-based compounds with high thermoelectric performance and ultralow lattice thermal conductivity *via* introduction of multiscale scattering centers. *Materiomics*, 10: 200-209. https://doi.org/10.1016/j.matt.2024.01.018

[17]. Omprakash M., Singh S., Hirata K., Kuga K., Harish S., Shimomura M., Adachi M., Yamamoto Y., Matsunami M. and Takeuchi T. (2021). Synergetic enhancement of power factor and suppression of lattice thermal conductivity via electronic structure modification and nanostructuring on Ni and B co-doped p-type Si-Ge alloy. *ACS Appl. Electron. Mater.*, 3: 5621–5631. https://doi.org/10.1021/acsaelm.1c01030

[18]. Yoon S.M., Dharmaiah P., Kim H.S., Lee Ch.H., Hong S.-J. and Koo J.M. (2017). Investigation of thermoelectric properties with dispersion of Fe_2O_3 and Fe-85Ni nanospheres in $Bi_{0.5}Sb_{1.5}Te_3$ matrix. *Electron. Mater.*, 46: 2770–2777. https://doi.org/10.1007/s11664-017-5353-4

[19]. Sharma V., Sharma D. and Bhatt R. (2022). Enhanced thermoelectric performance of nanostructured nickel doped Ag_2Te. *ACS Appl. Energy Mater*., 5: 13887–13894. https://doi.org/10.1021/acsaem.2c02562

[20]. Kwon H. and Kim I.-H. (2025). Effects of Ni doping on thermoelectric properties of chalcopyrite. *Materials*, 18: 2738. https://doi.org/10.3390/ma18082738

[21]. Kush L., Srivastava S., Jaiswal Y. and Srivastava Y. (2020). Thermoelectric behaviour with high lattice thermal conductivity of Nickel base $Ni_2CuCrFeAl_x$ (x = 0.5, 1.0, 1.5 and 2.5) high entropy alloys. *Mater. Res. Express*, 7: 035704. https://doi.org/10.1088/2053-1591/ab7c8a

[22]. Li Sh., Das S.S., Wang H., Bati S., Balachandran P.V., Shiomi J., Floroa J.A. and Zebarjadi M. (2025). High thermoelectric power factor in Ni-Fe alloy for active cooling applications. *Mater. Hor.*, 2025, Advance Article. https://doi.org/10.1039/D5MH00241E

[23]. Xiong Q., Wu H., Wang Gui., Zheng S., Feng Y., Wu Sh., Zhang B., Han G., Wang Guo., Zhou X. and Lu X. (2024). Realizing high thermoelectric performance and thermal stability in $CuInTe_2$ through heavy dose Mg doping. *Acta Materialia*,

278: 120268. https://doi.org/10.1016/j.actamat.2024.120268

[24]. Zhao D., Wang L., Bo L. and Wu D. (2018). Synthesis and thermoelectric properties of Ni-doped ZrCoSb half-Heusler compounds. *Metals, 8*: 61. https://doi.org/10.3390/met8010061

[25]. Wang Z.J. (2024). Enhanced thermoelectric transport properties of electronegative-element-filled and (Ni, Te) co-doped skutterudites through S filling $Sn_xNi_{0.4}Co_{3.6}Sb_{11.2}Te_{0.8}$. *Crystals, 14*: 728. https://doi.org/10.3390/cryst14070728

[26]. Kim S.I., Lee G.-E. and Kim I.-H. (2019). Thermoelectric properties of mechanically-alloyed and hot-pressed $Cu_{12-x}Co_xSb_4S_{13}$ tetrahedrites. *Korean Phys. Soc*., 74: 967-971. https://doi.org/10.3938/jkps.74.967

[27]. Qian X., Wang D., Zhang Y., Wu H., Pennycook S.J., Zheng L., Poudeu P.F.P. and Zhao L.-D. (2020). Contrasting role of small metallic elements (M=Cu, Zn, Ni) in enhancing the thermoelectric performance of n-type $PbM_{0.01}Se$. *Mater. Chem. A*, 8: 1-26. https://doi.org/10.1039/D0TA03251F

[28]. Guo X, Zhu W, Xiang L, et al. (2025),General screening rules and segmented optimization strategy for efficient thermoelectric devices.*Advanced Energy Materials* 15, 2402678. https://doi.org/10.1002/aenm.202402678

[29]. Sethuraman D.B.S. and Liu C.J. (2025). Energy-efficient synthesis and thermoelectric properties of $Ni_{1-x}Cr_x$ (x=0.08, 0.10 and 0.17) alloys. *Alloys and Comp*., 1010: 177569. https://doi.org/10.1016/j.jallcom.2024.177569

[30]. Yang X., Liu Yi., Min R., Jiang X., Liu Ya., Zhang Y. and Chen H. (2025). Synergetic band and defect engineering in ZrNiSn alloys via Ni-vacancy regulation for realizing high thermoelectric performance. *Acta Mater*., 284: 120626. https://doi.org/10.1016/j.actamat.2024.120626

[31]. Adamo C.G., Srivastava A., Kumar D., Legese S.Sh., Sreeram P.R., Mangalassery N.M. and Kawamura Y. (2025). Tailoring Ni/Fe doping for superior thermoelectric performance of $Zr_2Ni_{2-x}Fe_xSnSb$ (x=0.30, 0.35, 0.40) high-entropy alloys. *Energy Technol*., 13: 2401718. https://doi.org/10.1002/ente.202401718

[32]. Guo K., Zhang J., Zhang Y., Liu L., Yuan S., Jiang Y., Luo J. and Zhao J.-T. (2021). Minimizing thermal conductivity for boosting thermoelectric properties of Cu–Ni-based alloys through all-scale hierarchical architectures. *ACS Appl. Energy Mater*., 4: 5015–5023. https://doi.org/10.1007/s40843-023-2467-9

[33]. Wang Ch., Dong Z., Chen J., Zhili L., Gan L., Yang J., Zhang J. and Luo J. (2023). Structure and thermoelectric property evolution of $TiFe_{1.1-x}Ni_xSb$ with the filling of Ni. *Sci. China Mater.*, 66: 3230–3237. https://doi.org/10.1002/acle.202400003

[34]. Wang X., Tan X.Y., Ni X., Wang S., Chien Sh.W., Wuu D., Thitsartarn W., Lau D.K.B., Ye E., Ji R., Wang P. and Zhu Q. (2025). 3D printing elastocaloric TiNiCu thermoelectric shape memory alloys. *Asian Chem*., 20: e202400003. https://doi.org/10.1038/s41467-023-38166-5

[35]. Zhou Z., Huang Y., Wei B., Yang Y., Yu D., Zheng Y., He D., Zhang W., Zou M., Lan J.-L., He J., Nan C.-W. and Lin Y.-H. (2023). Compositing effects for high thermoelectric performance of Cu_2Se-based materials. *Nat. Commun*., 14: 2410. https://doi.org/10.1016/j.mtphys.2022.100795

[36]. Li Sh., Snyder K., Akhanda S., Martukanitz R., Mitra M., Poon J. and Zebarjadi M. (2022). Cost-efficient copper-nickel alloy for active cooling applications. *Heat and Mass Transfer*, 195: 123181. https://doi.org/10.1002/adma.202420556

[37]. Cherniushok O., Parashchuk T., Snyder G.J. and Wojciechowski K.T. (2025). Discovery of a new Cu-based chalcogenide with high *zT* near room temperature: Low-cost alternative for the Bi_2Te_3-based thermoelectrics. *Adv. Materials*, 37: 2420556. https://doi.org/10.1021/acssuschemeng.0c07329

[38]. Baláž P., Achimovičová M., Baláž M., Chen K., Dobrozhan O., Guilmeau E., Hejtmánek J., Knížek K., Kubíčková L., Levinský P., Puchý V., Reece M.J., Varga P. and Zhang R. (2021). Thermoelectric Cu–S-based materials synthesized via a scalabe mechanochemical process. *ACS Sustain. Chem. & Eng*., 9: 2003-2016. https://doi.org/10.1038/s41560-024-01572-4

[39]. Choo S., Lee J., Şişik B., Jung S.-J., Kim K., Yang S.E., Jo S., Nam Ch., Ahn S., Lee H.S., Chae H.G., Kim S.K., LeBlanc S. and Son J.S. (2024). Geometric design of Cu_2Se-based thermoelectric materials for enhancing power generation. *Nat. Energy*, 9: 1105-1116. https://doi.org/10.3390/ma16155204

[40]. Tie L., Xu G., Li Y., Fan X., Yang Q. and Nan B. (2023). Study on enhancing the thermoelectric stability of the β-Cu_2Se phase by Mn doping. *Materials*, 16: 5204. https://doi.org/10.1016/j.jallcom.2023.172615

[41]. Parvathy T. and Pradyumnan P.P. (2024). Impact of mobility and effective mass on the thermoelectric performance of Ni doped Cu_2Se. *Alloys and Comp*., 970: 172615. https://doi.org/10.1039/C8SC02011A

[42]. Shi X., Zheng K., Hong M., Liu W., Moshwan R., Wang Y., Qu X., Chen Z.-G. and Zou J. (2018). Boosting the thermoelectric performance of p-type heavily Cu-doped polycrystalline SnSe *via* inducing intensive crystal imperfections and defect phonon scattering. *Chemical Sci*., 37: 7376. https://doi.org/10.1016/j.mseb.2023.116961

[43]. Keddari H., Sahnoun O., Sahnoun M., Riane H. and El Houda Mokhfi N. (2024). The effect of Cu doping on the thermoelectric properties of $Cs_2Cu_xAg_{1-x}BiBr_6$ perovskites. *Materials Sci. and Engin.: B*, 299: 116961. https://doi.org/10.1016/j.matt.2023.11.009

[44]. Yang X., Ni H.,Yu X., Cao B., Xing J., Chen Q., Xi L., Liu, J., Zhang J., Guo K. and Zhao J.-T. (2024). Roles of concentration-dependent Cu doping behaviors on the thermoelectric properties of

n-type $Mg_3Sb_{1.5}Bi_{0.5}$. *Materiomics*, 10: 154-162. https://doi.org/10.1016/j.jallcom.2024.176908

[45]. Sivakumar M., Sidharth D., Srinivasan B. and Arivanandhan M. (2024). Improving thermoelectric performance of nickel substituted ZnSb alloy through carrier engineering and nanostructuring. *Alloys and Comp*., 1009: 176908. https://doi.org/10.1002/admi.202300705

[46]. Nasiri M.A., Seijas-da Silva A. and Claumarchirant J.F.S. (2024). Ultrathin transparent nickel electrodes for thermoelectric applications. *Adv. Mater. Iterfaces*, 11: 2300705. https://doi.org/10.3390/inorganics12030285

[47]. Fronzi M., Mele P. and Latronico G. (2024). Advances in thermoelectric materials - Bridging the gap between discovery and application. *Inorganics, 12*: 285. https://doi.org/10.1016/j.matdes.2023.112757

[48]. Deshpande R., Camut J., Müller E. and de Boor J. (2024). Device level assessment of Ni and $Ni_{45}Cu_{55}$ as electrodes in Mg_2(Si,Sn)-based thermoelectric generators. *Materials & Design*, 229: 112757. https://doi.org/10.3390/ma17081906

[49]. Galeano-Cabra J.R., Schundelmier B., Oladehi O. Feng K., Ordonez J.C., Baumbach R.E. and Wei K. (2024). Effect of Ni doping on the thermoelectric properties of $YbCo_2Zn_{20}$. *Materials*, 17: 1906. https://doi.org/10.1002/adfm.201903867

[50]. Zhao K., Qiu P., Shi X. and Chen L. (2020). Recent advances in liquid-like thermoelectric materials. *Adv. Funct. Mater.*, 30: 1903867. https://doi.org/10.3390/ma16051902

[51]. Sadia Y., Lumbroso D. and Gelbstein Y. (2023). Materials high-ZT due to the influence of copper in $Ti(Ni_{1-x}Cu_x)Sn$. *Materials*, 16: 1902. https://doi.org/10.3390/nano10050854

[52]. Hamawandi B., Ballikaya S., Råsander M., Halim J., Vinciguerra L., Rosén J., Johnsson M. and Toprak M.S. (2020). Composition tuning of nanostructured binary copper selenides through rapid chemical synthesis and their thermoelectric property evaluation. *Nanomaterials*, 10: 854. https://doi.org/10.1002/adfm.202411054

[53]. Zhang M., Shi X.-L., Mao Y., Li M., Moshwan R., Cao T., Chen W., Yin L., Lyu W., Chen Y., Liu S., Liu W.-D., Liu Q., Tang G. and Chen Z.G. (2024). High-performance GeSe-based thermoelectrics via Cu-doping. *Adv. Funct. Materials*, 34: 2411054. https://doi.org/10.1063/1.4896482

[54]. Qin Y., Yang L., Wei J., Yang S., Zhang M., Wang X. and Yang F. (2020). Doping effect on Cu_2Se thermoelectric performance: A review. *Materials*, 13: 5704. https://doi.org/10.1007/s11664-020-07999-6

[55]. Zhong B., Zhang Y., Li W., Chen Z., Cui J., Li W., Xie Y., Hao Q. and He Q. (2014). High superionic conduction arising from aligned large lamellae and large figure of merit in bulk $Cu_{1.94}Al_{0.02}Se$. *Appl. Phys. Lett.*, 105: 123902. https://doi.org/10.1126/sciadv.abc0726

[56]. Zhou Z., Huang Y., Wei B., Yang Y., Yu D., Zheng Y., He D., Zhang W., Zou M., Lan J.-L., He J., Nan C.-W. and Lin Y.H. (2023). Compositing effects for high thermoelectric performance of Cu_2Se-based materials. *Nat. Commun*., 14: 2410. https://doi.org/10.1557/PROC-793-S2.3

[57]. Guo X., Zhu, W., Xiang, L., Mu, S., Li, C., Ma, Sh., Wei, P., Nie, X., Zhang, Q. and Zhao, W. (2020). Preparation and characterization of $Ni/Bi_{0.5}Sb_{1.5}Te_3$ heterogeneous multilayered thermoelectric materials. Electron. Mater., 49(5), 2689–2697. https://doi.org/10.1063/1.1689399

[58]. Zhang X., Bu Z., Shi X., Lin S., Shan B., Wood M., Snyder A.H., Chen L. and Pei Y. (2020). Electronic quality factor for thermoelectric. *Sci. Adv*., 6: eabc0726. https://doi.org/10.1016/j.mtener.2024.101564

[59]. Snyder G.J. and Caillat T. (2003). Using the compatibility factor to design high efficiency segmented thermoelectric generators. *MRS Proc. Libr*., 793: 37. https://doi.org/10.1557/PROC-793-S2.3

[60]. Snyder G.J. (2004). Application of the compatibility factor to the design of segmented and cascaded thermoelectric generators. *Appl. Phys. Lett.*, 84: 2436. https://doi.org/10.1063/1.1689399

[61]. Lobato C.N., Esposito V., Pryds N. and Christensen D.V. (2024). How efficient are thermoelectric materials? – An assessment of state-of-the-art individual and segmented thermoelectric materials. *Materialstoday-Energy*, 43: 101564. https://doi.org/10.1016/j.mtener.2024.101564

[62]. Idogho C., Abah E.O., Imbur T., Omenka K., Idoko P.I. (2025).Numerical simulation and synthesized material ranking for high-temperature thermoelectric power generation.*Energy Technology*.https://doi.org/10.1002/ente.202502104

[63]. Nurachman A., Permata S., Idogho Ch., Harsito C., Ilogho T. and Abel Ejila J. (2025). Compatibility in thermoelectric material synthesis and thermal transport. *Unconvent. Resources*, 7: 100198. https://doi.org/10.1016/j.unconv.2025.100198

[64]. Christian I., Abah E.O., Abel J.E., Harsito C., Omoniyi M. and Boriwaye T. (2025). Compatibility study of synthesized materials for thermal transport in thermoelectric power generation. *Innovat. Sci. and Engineering*, 4: 2158-7205. https://doi.org/10.48084/iset.2025.21587205

[65]. Xiong Q, Wu H, Wang G, et al. (2024),High thermoelectric performance and thermal stability in $CuInTe_2$ via heavy Mg doping.*Acta Materialia* 278, 120268. https://doi.org/10.1016/j.actamat.2024.120268

[66]. Sagar A., Bhardwaj A., Novitskii A., Khovaylo V. and Patnaik S. (2024). Substantial enhancement in thermoelectric figure-of-merit of half Heusler ZrNiPb alloys. *Bull. Materials Sci*., 47: 0146. https://doi.org/10.1007/s12034-024-03146-0

[67]. Idogho C (2025).High-temperature performance of Ho–Sb–Te thermoelectrics: substrate compatibility and geometry-driven efficiency optimization.*Energies* 18:3124. https://doi.org/10.3390/en18123124

[68]. Min R, Wang Y, Jiang X, et al. (2024),ZrNiSn-based compounds with high thermoelectric performance and ultralow lattice thermal conductivity.*Materiomics* 10, 200–209. https://doi.org/10.1016/j.matt.2024.01.018

[69]. Mishra S-R, Tan L-P, Trivedi V, et al. (2023),Low lattice thermal conductivity in Zr-doped $Ti_2NiCoSnSb$ thermoelectric alloys.*ACS Applied Energy Materials* 6, 6262–6277. https://doi.org/10.1021/acsaem.3c00887

[70]. Lobato C-N, Esposito V, Pryds N, Christensen D-V (2024),How efficient are thermoelectric materials.*Materials Today Energy* 43, 101564. https://doi.org/10.1016/j.mtener.2024.101564

[71]. Zhang X, Bu Z, Shi X, et al. (2020),Electronic quality factor for thermoelectrics.,*Science Advances* 6, eabc0726. https://doi.org/10.1126/sciadv.abc0726

[72]. Shi X, Zheng K, Hong M, et al. (2018),Boosting thermoelectric performance of p-type heavily Cu-doped polycrystalline SnSe.*Chemical Science* 9, 7376–7389. https://doi.org/10.1039/C8SC02011A

[73]. Zhang M, Shi X-L, Mao Y, et al. (2024),High-performance GeSe-based thermoelectrics via Cu doping. *Advanced Functional Materials* 34, 2411054. https://doi.org/10.1002/adfm.202411054

[74]. Mishra S.R., Karati A., Ghosh S., Mallik R.Ch., Shabadi R., Krishnan S.R., Yadav S., Ramanujan R.V., Murty B.S. (2023).Lowering thermal conductivity in thermoelectric $Ti_{2-x}NiCoSnSb$ half-Heusler high-entropy alloys.*Materials Science and Engineering: B* 58, 10736. https://doi.org/10.1016/j.mseb.2023.116489

[75]. Feng Y., Joo J.H., Han G., Lu N. (2023).The effect of Fe addition for enhanced thermoelectric performance in p-type $CuAl_{0.8}Fe_{0.2}O_2$.*Engineered Science* 22, 822. https://doi.org/10.30919/es.2023.822

[76]. Abah, E. O., & Idogho, C. (2026). Machine-Learning-Based Mapping and Ranking of Energy Materials in African Economies. *European Journal of Science, Innovation and Technology*, *6*(1), 15-32. Retrieved from https://ejsit-journal.com/index.php/ejsit/article/view/738

[77]. Idogho, C., Abah, E. O., Imbur, T., & Omenka, K. (2026). Intrinsic Electronic Quality and Compatibility-Factor-Driven Design of Thermoelectric Materials Across Temperature Regimes. *International Journal of Scientific Research and Modern Technology*, *5*(1), 110–127. https://doi.org/10.38124/ijsrmt.v5i1.1169

[78]. C. Maduabuchi, C. Nsude, C. Eneh, E. Eke, K. Okoli, E. Okpara, C. Idogho, B. Waya, C. Harsito, Renewable Energy Potential Estimation Using Climatic-Weather-Forecasting Machine Learning Algorithms, Energies. 16 (2023). https://doi.org/10.3390/en16041603

[79]. I. Idoko, G. Ezeamii, I. Christian, E. Peter, U. Obot, V. Iguoba, Mathematical modeling and simulations using software like MATLAB, COMSOL, and Python, Magna Sci. Adv. Res. Rev. 12 (2024) 62–95. https://doi.org/10.30574/msarr.2024.12.2.0181